Development and regeneration of hair cells share common functional features

Snezana Levic*, Liping Nie*, Dipika Tuteja†, Margaret Harvey‡, Bernd H. A. Sokolowski‡, and Ebenezer N. Yamoah*§

*Department of Otolaryngology, Program in Communication Science, Center for Neuroscience, University of California, 1544 Newton Court, Davis, CA 95616; †Division of Cardiology, Department of Medicine, University of California, 2315 Stockton Boulevard, Sacramento, CA 95817; and ‡Otology Laboratory, Department of Otolaryngology, University of South Florida, MDC83, 12901 Bruce B. Downs Boulevard, Tampa, FL 33612

Edited by Edward G. Jones, University of California, Davis, CA, and approved October 11, 2007 (received for review June 26, 2007)

The structural phenotype of neural connections in the auditory brainstem is sculpted by spontaneous and stimulus-induced neural activities during development. However, functional and molecular mechanisms of spontaneous action potentials (SAPs) in the developing cochlea are unknown. Additionally, it is unclear how regenerating hair cells establish their neural ranking in the constellation of neurons in the brainstem. We have demonstrated that a transient Ca^{2+} current produced by the $Ca_v3.1$ channel is expressed early in development to initiate spontaneous Ca^{2+} spikes. $Ca_v1.3$ currents, typical of mature hair cells, appeared later in development. Moreover, there is a surprising disappearance of the $Ca_v3.1$ current that coincides with the attenuation of the transient Ca^{2+} current as the electrical properties of hair cells transition to the mature phenotype. Remarkably, this process is recapitulated during hair-cell regeneration, suggesting that the transient expression of $Ca_v3.1$ and the ensuing SAPs are signatures of hair cell development and regeneration.

Ca^{2+} currents | cochlea | hearing | spontaneous activity

In the developing nervous system, patterned spontaneous action potentials (SAPs) play an instructive role in the survival and refinement of neuronal connections before stimulus-induced activity (1). In the auditory setting, hair cells (HCs) fire SAPs before the onset of hearing, a period when major synaptic refinement occurs within the cochlea and cochlear nucleus (CN) (2). Indeed, transneuronal pruning in the CN depends on spontaneous activity (SA) of HCs during development, and the activity of the VIIIth nerve is required for neuronal survival in the mature CN (3). This dynamic plasticity raises the possibility that newly regenerated HCs in the mature cochlea must assume a distinct functional phenotype by acquiring both appropriate ion channels for signal processing and VIIIth nerve synapses to establish their connectivity and ranking in the CN. Studies of HC regeneration in the inner ear of birds have demonstrated unequivocally that there is recovery of both electrical responses in the CN and behavioral responses to sound (4). However, the mechanism whereby newborn HCs acquire their functionality and connectivity in the CN is unknown.

Beyond these uncertainties, it is also unclear whether neural activity recorded from the CN during development is patterned. There appears to be a stark correlation between the rate of ordered rhythmic bursting and the tonotopic position of neurons in the CN (5, 6). In contrast to Na^+ spikes in the developing visual system, SA in prehearing HCs is derived mainly from Ca^{2+} spikes (7, 8). Ca^{2+}-mediated action potentials (APs) and the ensuing increase in intracellular Ca^{2+} may induce the release of neurotrophins (9), mediate the expression of K^+ channels that attenuate SAPs in HCs, and/or activate genes that may refine neuronal connections (10).

Hair cells express multiple Ca^{2+} channels. However, only the $Ca_v1.3$ channels and their functional roles have been identified decisively in posthearing HCs (11–13). Meanwhile, in cochlear HCs, the $Ca_v1.3$ current alone does not suffice to account for the total Ca^{2+} current (14), and the identity of the non-$Ca_v1.3$ current remains elusive. Here, in the developing chicken cochlea, we have shown that $Ca_v3.1$ is expressed as early as embryonic day 7 (E7) to initiate SAPs before most neuronal connectivity is established. $Ca_v1.3$, the predominant Ca^{2+} channel in posthearing HCs, appeared later at ≈E12. Surprisingly, the $Ca_v3.1$ disappeared as the electrical properties of HCs transitioned to maturity. Furthermore, the process is recapitulated during regeneration of HCs, suggesting that SA may be necessary for the maturation of HCs and that the expression of $Ca_v3.1$ is a developmental and regenerative signature of HCs.

Results

Functional Changes in Whole-Cell Ca^{2+} Currents in Hair Cells During Development. We examined Ca^{2+} currents from developing HCs in the chicken basilar papilla by suppressing outward K^+ currents. The Ca^{2+} current was visibly altered from E7 to postnatal day 2 (P2) in three ways. Fig. 1*A* shows traces of the Ca^{2+} current from the earliest ages examined (E7), when terminal differentiation of HCs is completed (15). In stark contrast to Ca^{2+} currents from posthatched HCs (16), the currents at E7–E12 showed a prominent decay over a 50-ms-duration voltage step. We recognized the possibility that activation of outward current might contaminate the Ca^{2+} current, resulting in the apparent decay. However, this was not the case. As shown in Fig. 1*B*, the current traces generated by step potentials at −10 mV decayed faster than traces elicited at 30 mV, indicating that the inactivation of the Ca^{2+} current was genuine. Fig. 1 *C* and *D* summarizes the current magnitude and density–voltage relationship at different stages of development. There was a minimum of a 3-fold increase in the current magnitude from E7 to E16 before the size of the current plummeted by ≈1.5-fold. Moreover, because of the apparent increase in HC membrane area during development (17), the current–density peaked at E12 with a subsequent 2-fold down-regulation by P2. Last, HCs, which expressed Ca^{2+} currents with a transient component, were present throughout the basilar papilla at all stages of development (Fig. 1*E*). The magnitude of the transient current showed a marked decline at ≈E16 and beyond. The half-activation voltage ($V_{1/2}$) was shifted by ≈8 mV for currents recorded at E10 compared with those recorded at E12–P2 (Fig. 1*F*). $V_{1/2}$ of the steady-state inactivation curve was approximately −37 mV. A window current became apparent from the crossovers of the activation and inactivation curves, suggesting that the transient current may be partially activated at rest.

These findings served as a backdrop against which we used to correlate the functional development of HCs and their synaptic connectivity, while also attempting to reconcile Ca^{2+} currents in developing and posthatched HCs. The birth of the transient current precedes the establishment of any observed matured-like synaptic

Author contributions: E.N.Y. designed research; S.L., L.N., D.T., M.H., B.H.A.S., and E.N.Y. performed research; D.T. contributed new reagents/analytic tools; S.L., L.N., B.H.A.S., and E.N.Y. analyzed data; and E.N.Y. wrote the paper.

The authors declare no conflict of interest.

This article is a PNAS Direct Submission.

§To whom correspondence should be addressed. E-mail: enyamoah@ucdavis.edu.

This article contains supporting information online at www.pnas.org/cgi/content/full/0705927104/DC1.

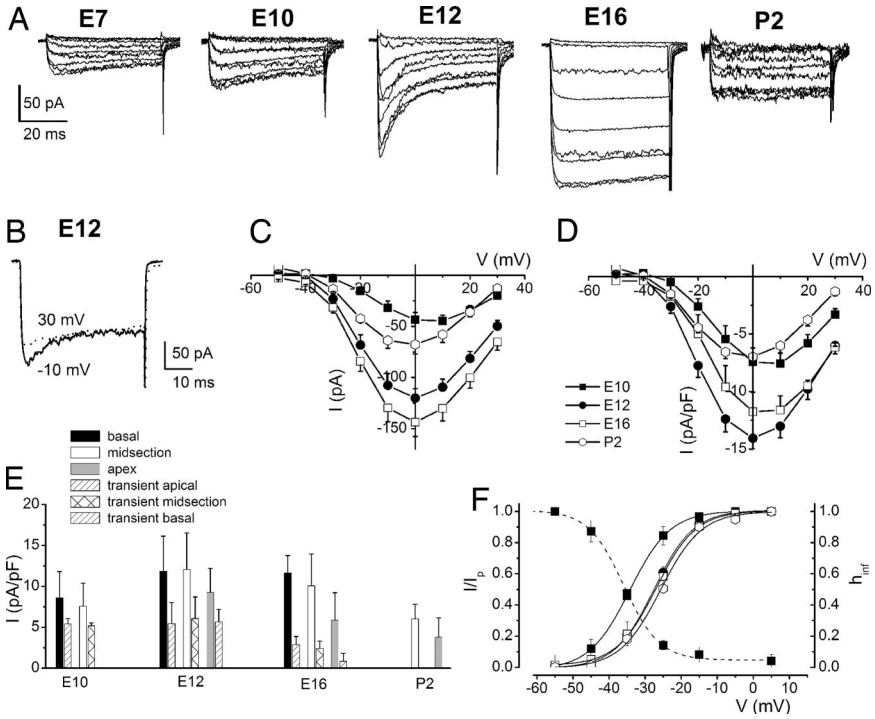

Fig. 1. Changes in profiles of Ca^{2+} currents at different stages of development (*A*) Examples of current traces recorded at E7, E10, E12, E16, and P2 from the midsection of basilar papilla. Currents were elicited by 50-ms depolarizing voltage steps in 10-mV increments from a holding potential of −90 mV. (*B*) Shown are two traces from E12 that were elicited at step potentials of −10 mV (solid line) and 30 mV (dotted line). The decay of the current traces was more pronounced at more negative step potentials than at positive step potentials. (*C*) Note the increase in current amplitude during development, which peaked at ≈E16. (*D*) Plots of the mean peak current densities show that current density reached maximum at E12. (*E*) Mean current density at 0 mV at apical, midsection, and basal regions of the basilar papilla (pA/pF) at E10, E12, E16, and P2. The transient current amplitude increased early in development until E12 and decreased at more mature stages. E10, $n = 19$; E12, $n = 53$; E16, $n = 36$; P2, $n = 9$ cells. (*F*) The Boltzmann fits are plotted with solid lines. Half-activation voltages (in mV) were -34.2 ± 1.1, -27.5 ± 0.3, -26.9 ± 0.2, and -25.7 ± 0.8 for currents at E10, E12, E16, and P2, respectively. The maximum slope factors for the activation curves (in mV) were 5.4 ± 0.6, 5.5 ± 0.3, 5.8 ± 0.3, 5.6 ± 0.8 ($n = 15$) for currents recorded at E10, E12, E16, and P2, respectively. Steady-state inactivation of Ca^{2+} currents was determined at E10. The half-inactivation and slope factors were -36.7 ± 1.4 and 4.9 ± 2.0 ($n = 14$), respectively. Overlap of the steady-sate activation and inactivation curves at a voltage range of −60 to −40 mV suggests that the Ca^{2+} current is active at the apparent resting membrane potential of developing hair cells.

contacts (18), the onset of mechanoelectrical transduction (17), and synaptic transmission (19). From this baseline, we considered segregating the transient and sustained components of the Ca^{2+} currents. The transient current was remarkably sensitive to holding voltages. As illustrated in Fig. 2*A*, Ca^{2+} currents elicited from a holding potential of −90 mV showed an increase in amplitude and prominent inactivation compared with currents elicited at a holding potential of −50 mV. The difference current, which is chiefly the transient component, was readily activated at −90 mV but was inaccessible for activation at the −50-mV holding voltage. The simplest explanation for these findings is that, at E12, HCs express at least two different classes of Ca^{2+} currents, with the transient component declining as HCs mature. At E12, $63 \pm 25\%$ ($n = 9$) of the total current constituted the transient current, but by E16, the transient component had declined to $23 \pm 9\%$ ($n = 9$) of the total current. In contrast, mature HCs (P2) showed no noticeable differences in currents elicited from −90- and −50-mV holding voltages (Fig. 2*B*). Because the voltage-dependent properties of the transient current remarkably mirrored features of T-type Ca^{2+} currents, we examined the sensitivity of the current to T-type Ca^{2+} channel blockers (20, 21). From a holding potential of −90 mV to a step potential of −10 mV, kurtoxin suppressed a sizable portion of the transient current at E12. At P2, kurtoxin unmasked a miniature transient component of the whole-cell Ca^{2+} current that was otherwise unappreciated (Fig. 2 *C* and *D*). Similarly, application of mibefradil and nickel suppressed the transient Ca^{2+} current in developing HCs [supporting information (SI) Fig. 6]. Fig. 2*E* illustrates the striking agreement between magnitudes of the kurtoxin- and holding-potential-sensitive currents (SI Fig. 6). The half-blocking concentration of kurtoxin was 38 ± 4 nM (Fig. 2*F*).

Kinetics of activation and inactivation of the transient and sustained currents were examined for E12–P2 HCs. Consistent with the assertion that there are multiple components of Ca^{2+} currents in developing HCs, the kinetics of activation/deactivation (SI Fig. 7) and inactivation of these currents varied (SI Fig. 8). The time constants of inactivation (τ_I) were compared at different stages of development. At the embryonic stages tested (E10–E16), the kinetics of decay of the current were fitted with three time constants. However, at P2, one τ_I was sufficient to fit the decay profile. We also examined the time dependence of development and recovery from inactivation after various durations of current at −50 and −90 mV (SI Fig. 8). In contrast to Ca^{2+} currents at E12, at P2 and beyond, the current was steady and showed little to no recovery from inactivation after a 3-second test pulse. Thus, the functional data suggests that the inactivation of the Ca^{2+} current is labile; although prominent at early stages in HC development, it is reduced at later stages.

Reappearance of Transient Ca^{2+} Current and Spontaneous Spikes During HC Regeneration. The promise for HC regeneration in the mammalian cochlea has been demonstrated. However, for a regenerated HC to function well in the mature cochlea, it must express the appropriate ionic currents and make correct synaptic contacts. To determine how a regenerated HC establishes its functional niche in the mature cochlea, we used the ability of adult chickens to regenerate HCs after the loss of original HCs due to

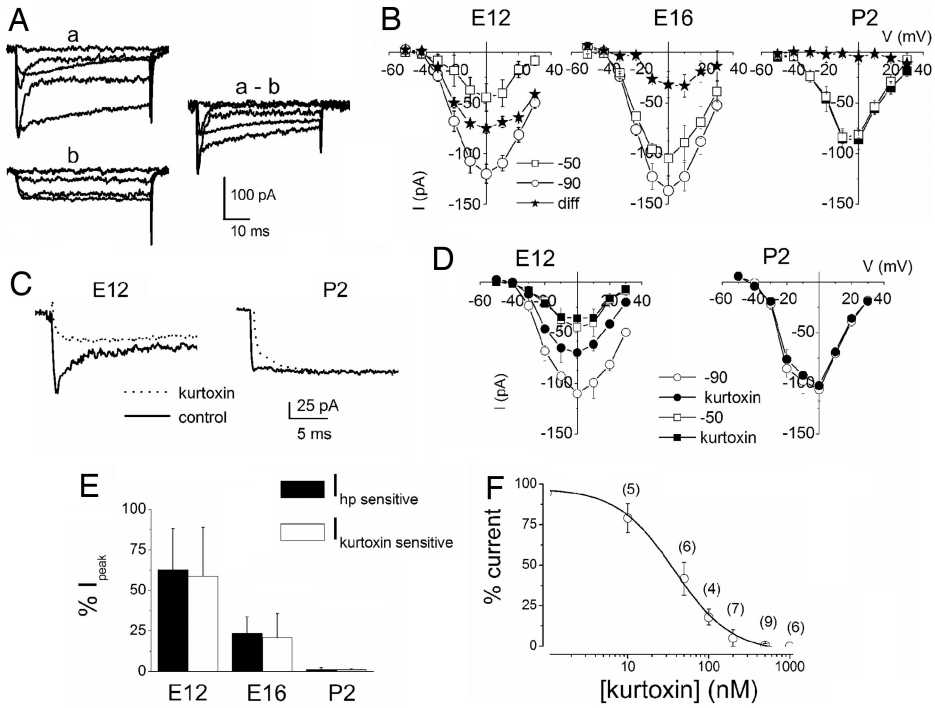

Fig. 2. Early in development, the Ca^{2+} current profile showed high sensitivity to holding potentials and kurtoxin. (*A*) (*a* and *b*) Current traces were obtained from E12 HCs. The current amplitude was larger, and currents had pronounced inactivation from the holding potential of −90 mV (*a*) than at −50 mV (*b*). (*a-b*) The difference current reflects the transient component of the whole-cell Ca^{2+} current. (*B*) Current–voltage (I–V) relationship of the peak current amplitude at −90 and −50 mV and the difference current at E12, *n* (cells) = 32; E16, *n* = 26; and P2, *n* = 9. (*C*) Kurtoxin, reduced the amplitude of Ca^{2+} current elicited from a holding potential of −90 mV only in early development. The current traces were elicited at a step potential of −10 mV before and after application of 300 nM kurtoxin. Control traces are shown in solid lines, and the kurtoxin-insensitive current traces are shown in dotted lines. The effect of kurtoxin was less pronounced on Ca^{2+} currents recorded at P2. A small transient current component at P2 was made apparent by the toxin. (*D*) The I–V relationship of currents at E12 and P2 showing their sensitivity toward kurtoxin: E12, *n* = 21; P2, *n* = 5. (*E*) Histogram showing that the holding potential (hp)-sensitive current was similar in magnitude to the kurtoxin-sensitive current. Additionally, the magnitude of the hp- and kurtoxin-sensitive current plummeted during development (*n* = 9). (*F*) Kurtoxin block of the transient Ca^{2+} current was dose-dependent. The half-blocking concentration and Hill coefficient of kurtoxin were estimated to be ≈38 ± 4 nM and 1.2, respectively.

ototoxic drug exposure (22). A single dose of gentamicin treatment (23) induced HC loss at the basal one-third of chicken cochlea, which was confirmed by scanning electron microscopy (data not shown). In contrast to mature HCs, newly regenerating cells expressed a transient Ca^{2+} current, evocative of the current found in the developing HCs (Fig. 3*A*). This transient current, which was sensitive to membrane holding voltage, was prominent in regenerating HCs 7 days after posttreatment (PT7). At PT7, the transient current formed 81 ± 6% (n = 7) of the total inward Ca^{2+} current, but it subsequently attenuated at PT15 (60 ± 3%, n = 9), PT25 (13 ± 8), and PT40 (5 ± 2%, n = 7) (Fig. 3 *B–E*). The return and further disappearance of the transient Ca^{2+} current in the regenerative process was indicative of a temporal-specific function.

To establish functional correlations, we tested the role of the transient Ca^{2+} current in the generation of SAPs as T-type currents impact rhythmic spike activity in neurons (24). Hints of spike activity have been confirmed and the generation of primordial SAPs in chicken HCs has been inferred (25). However, SAPs in the developing mammalian HC have been demonstrated unequivocally (8). We determined the exact time of SAP initiation in the developing chicken HCs. Sporadic SAPs were detected as early as E7.5. Furthermore, by E8, robust and reliable spike activity ensued, reaching peak frequency at E12, then declining until attenuation at ≈E18. Fig. 4 *A* and *B* illustrates and quantifies these results. If the transient Ca^{2+} current contributes to the generation of SAPs, kurtoxin should thwart spike activity in the developing HC (SI Fig. 9). The effects of kurtoxin, Ni^{2+} and mibefradil on spike frequency and AP profile were marked (Fig. 4 *F* and *H* and SI Fig. 9). By P2, neither SAPs nor injected current were sufficient to evoke APs in HCs (Fig. 4*D*). To examine the effects of Ca^{2+} on SAPs and to preserve intracellular constituents, perforated patches were used to record APs. Whereas spike activities ceased in the absences of external Ca^{2+}, increased Ca^{2+} produced enhanced spike amplitude (SI Fig. 10). These observations underpin the importance of Ca^{2+} currents and intracellular Ca^{2+} in the regulation of APs in the developing HCs. Even so, tetrodotoxin (TTX), a potent blocker of Na^{+} channels, eliminates impulse firings in the developing CN that have been inferred to originate from the cochlea (5), although Na^{+} currents have been recorded from vestibular HCs (26). We tested the effects of TTX on spike activity and profile. As illustrated in Fig. 4 *E* and *I*, the effects of a sufficiently high concentration of TTX (1 μM) on spike activity and AP shape were not striking. This observation is in keeping with reports from developing mammalian HCs (8). To determine whether cochlear HCs in chickens expressed Na^{+} currents, we used conditions similar to that described in ref. 26. Using a holding voltage of −120 mV, we did not detect Na^{+} current in 45 cells sampled from chicken cochlear HC. The pattern of SAPs varied from tonic to burst discharge, as illustrated in SI Fig. 11. As shown in SI Fig. 12, the trend of firing switched from a tonic to a phasic pattern during development, showing an increase in burst duration and the number of spikes per burst from E8 to E16.

To consider the import of the transient Ca^{2+} current in development, another strategy was to determine whether its reappearance alone in the regenerating HCs was sufficient to induce SAPs. We first determined whether SAPs are also a feature of regenerating HCs. Regenerating HCs at the basal one-third of the cochlea elicited SAPs 7 days after gentamicin treatment (Fig. 4*F*). By contrast, HCs at the apical two-thirds of the cochlea, impervious to

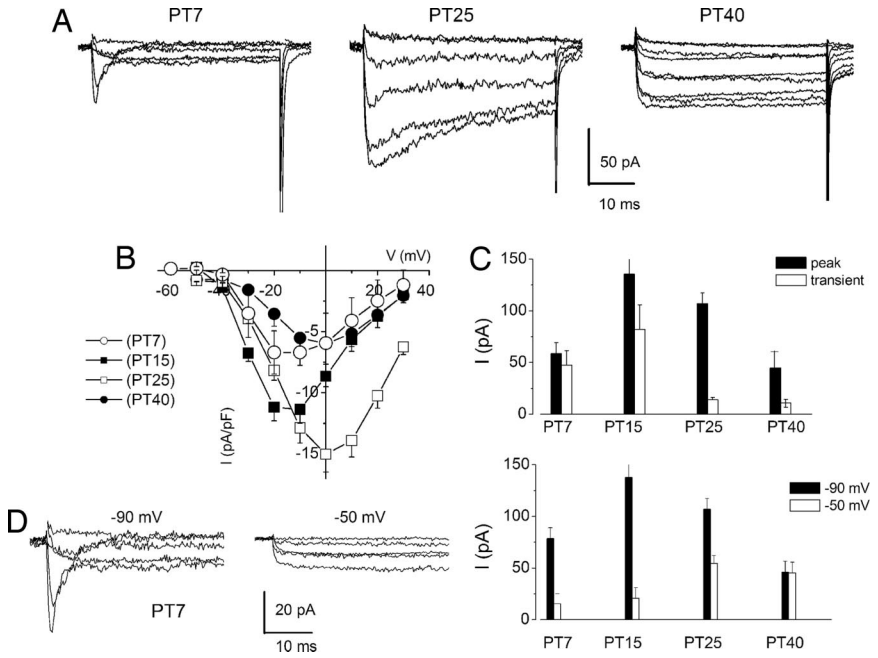

Fig. 3. The transient Ca^{2+} current reappears during hair cell regeneration. (*A*) Traces of Ca^{2+} currents at different posttreatment days (PT7, PT25, and PT40) of regenerating hair cells after gentamicin-induced hair cell death at the basal portion of the basilar papilla. The current traces were elicited with 50-ms depolarizing voltage steps in 10-mV increments from a holding potential of −90 mV. Ca^{2+} currents underwent the most dramatic changes between ≈PT7 and PT40. There was the appearance of a transient current followed by a sustained current and, later, the disappearance of the transient component. (*B*) Mean peak current density ± SD. (PT7, $n = 7$; PT15, $n = 9$; PT25, $n = 6$; PT40, $n = 7$). (*C*) Histogram showing the magnitude of the peak current at different days after gentamicin treatment and the estimated transient current. (*D*) The current amplitude was larger and had pronounced inactivation from the holding potential of −90 mV (*Left*) than at −50 mV (*Right*). (*E*) Summary data of the holding potential-sensitive peak currents at different stages after gentamicin treatment.

gentamicin-treatment, were quiescent and responded with membrane oscillations only to positively evoke current (data not shown), which is reminiscent of mature HCs (27). Indeed, by 40 days after gentamicin treatment, HCs at the basal one-third of the cochlea (regenerating HCs) ceased to generate SAPs (Fig. 4*G*). Because SAPs are recapitulated in the regenerating HCs, we assessed whether the transient Ca^{2+} current contributes toward SAPs on the basis of the current's sensitivity to kurtoxin and mibefradil. Fig. 4*F* and SI Fig. 9 demonstrate the transient Ca^{2+} current blockers' suppression of spike activity in the regenerating HCs, giving further credence to the importance of the current in the generation of SAPs in HCs.

Molecular Evidence for Transient Expression of a Ca_v3 Channel. To probe the molecular identity of the transient Ca^{2+} channel, first we used an RT-PCR approach to examine mRNA expression of a T-type Ca^{2+} channel, $Ca_v3.1$, in the chicken cochlea. Two different transcripts of $Ca_v3.1$ were detected at E8, E12, and E16, whereas only one major transcript was detected for P1 (SI Fig. 13). Sequence analysis revealed a 141-bp exon of $Ca_v3.1$ that introduces 47 aa to the proximal carboxyl terminus of the long isoform of the channel. Second, we used quantitative PCR methods to determine the levels of expression of the $Ca_v3.1$ longitudinally during development (Fig. 5*A*). *In situ* hybridization analysis revealed that the overall expression of $Ca_v3.1$ mRNA had a marked reduction pattern during development (Fig. 5*B*).

Discussion

We have demonstrated an important functional feature that exists in both developing and regenerating HCs. The findings established by this study not only deepen our mechanistic understanding of the critical import of primordial rhythmic electrical activity in developing HCs but also bring to light previously unidentified, yet significant, common features of the regenerating HC that may be relevant for maturity. In addition, before these studies, there was ample circumstantial evidence implicating Ca^{2+} channels besides $Ca_v1.3$ as minor players in multiple Ca^{2+}-dependent functions in HCs (28, 29), although the exact role of the non-$Ca_v1.3$ remained obscure. We have established that, indeed, a Ca^{2+} channel encoded by $Ca_v3.1$ is expressed in developing HCs to promote SAPs. A previous report made reference to the presence of a transient Ca^{2+} current in vestibular HCs (30). SI Table 1 compares the properties of the T-type Ca^{2+} current in HCs with currents in other systems. The resurfacing of the transient Ca^{2+} current and SAPs during regeneration of HCs is strong correlative evidence that the current is a prime contributor to SAPs in HCs. Indeed, the pharmacology of the transient Ca^{2+} current and attenuation of SAPs in the developing and regenerating HCs by T-type Ca^{2+} current-specific blockers affirms this assertion. Finally, and perhaps most compelling, is the realization that expression of the transient Ca^{2+} current predates the commencement of SAPs, whereas the expression of the $Ca_v1.3$ is detectable later in development. Nonetheless, the importance of the L-type current as an adjuvant to the T-type current at later stages of embryonic development (e.g., E16) should not be underrated. From this foothold, our study has uncovered a feature of the underlying basis for SAPs in developing and regenerating HCs, while establishing a functional attribute to a non-$Ca_v1.3$ channel. We suggest that the T-type Ca^{2+} current promotes SAPs in the developing and regenerating HCs to mediate activity-dependent developmental events in the auditory setting. Here, we elaborate on the implications of T-type Ca^{2+} current-mediated primordial Ca^{2+} spikes in HCs.

The fleeting expression of the T-type Ca^{2+} current strongly suggests that it serves a developmental function. Although a previously undescribed finding in the auditory setting, the decline or disappearance of T-type Ca^{2+} currents has been shown in early development of spinal and vestibular neurons among others (31–33). In developing HCs there was a remarkable correlation between

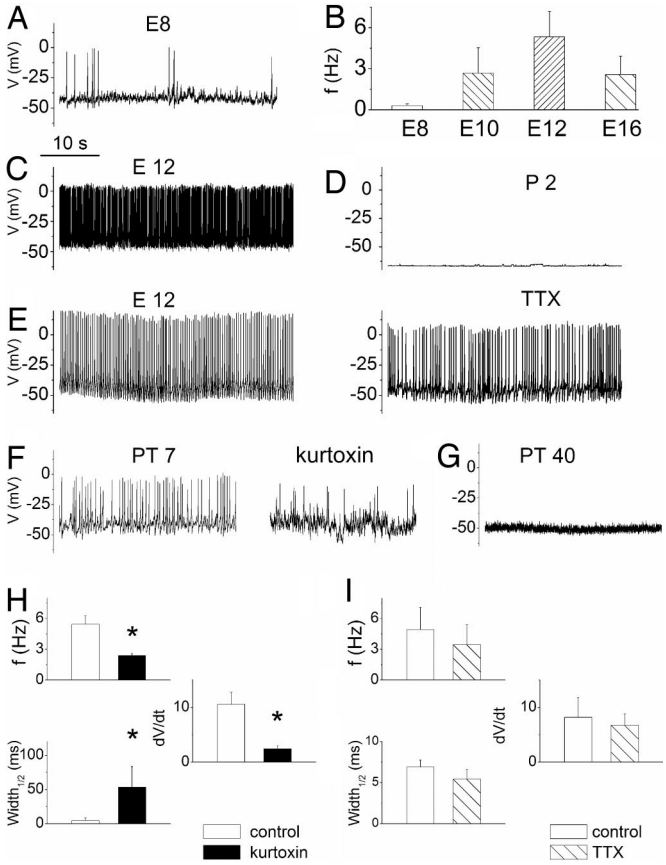

Fig. 4. Spontaneous action potentials in developing and regenerating hair cells. (*A*) Shown is an example of electrical activity observed in E8 hair cells. (*B*) Summary data on the frequency of firing at different stages of development (E8–E16, $n = 9$ cells). (*C*) An example of tonic discharge in an E12 hair cell. (*D*) In contrast to embryonic (prehatched) hair cells, posthatched hair cells (P2) were quiescent. (*E*) The effects of TTX on spontaneous action potentials were not marked [control (*Left*) and effect of 1 μM TTX (*Right*)]. (*F*) (*Left*) SAPs in a regenerating hair cell after 7-day gentamicin posttreatment (PT7). (*Right*) Similar to spontaneous electrical activity in the developing hair cell (SI Fig. 9), kurtoxin (300 nM) produced a marked reduction in spike activity. (*G*) Forty days after gentamicin treatment, regenerated hair cells assume the baseline quiescent electrical phenotype. (*H*) Summary data on the effects of kurtoxin (300 nM) on spike frequency (f), spike width, and rate of change of voltage of the depolarizing phase of spikes at E12. (*I*) Summary data on the effects of TTX (1 μM) on properties of SAPs and APs at E12. In addition, the effects of TTX on spike frequency (Hz) at PT7 were 2.3 ± 1.1 (control), and after TTX were 2.2 ± 1.3 ($n = 4$, $P = 0.6$). Comparisons that were statistically significant ($P < 0.05$) are indicated in asterisks.

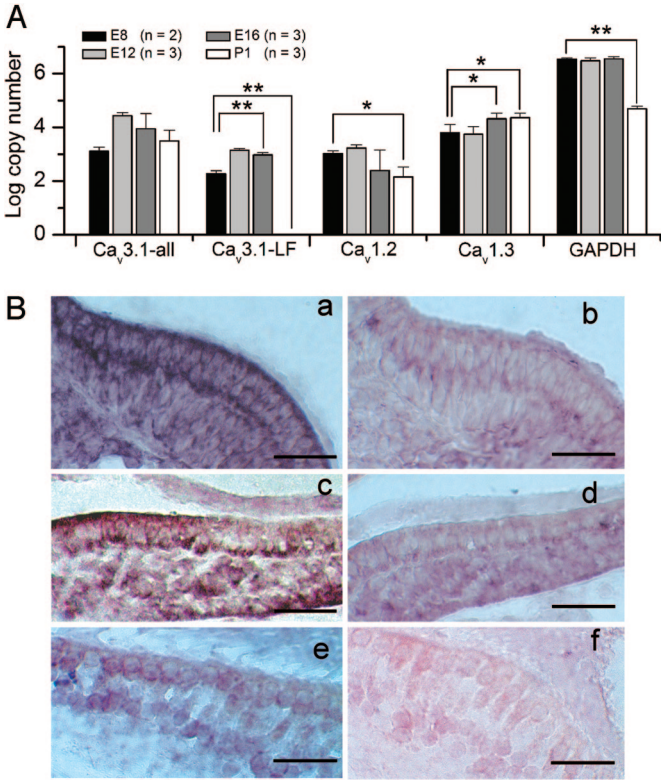

Fig. 5. Molecular identification of Ca_v channels in developing hair cells. (*A*) Quantitative analyses of expression for Ca_v channels were performed using real-time RT-PCR technique. The absolute copy number of transcripts per micrograms of total RNA for each primer pair was calculated from a corresponding standard curve obtained from the same plate and was plotted as the mean values (± SEM) from three individual experiments ($n = 3$). $Ca_v3.1$-all, all $Ca_v3.1$ transcripts; $Ca_v3.1$-LF, specific for the longer transcript. P values <0.05 were considered statistically significant compared with E8. *, $P < 0.05$; **, $P < 0.01$. The levels of $Ca_v1.2$ remained steady at E8–E16 until it declined at P1. (*B*) Distribution of $Ca_v3.1$ mRNA during different stages of chick cochlea development as revealed by *in situ* hybridization. (*a* and *c*) $Ca_v3.1$ mRNA appeared as early as E10 (*a*) and continued on into E16 (*c*). (*e*) However, the expression decreases by P3. (*b*, *d*, and *f*) Controls using sense probes are shown. (Scale bars, 50 μm.)

the temporal expression of the transient Ca^{2+} current and the emergence of SAPs. The partial blockage of the transient Ca^{2+} current alone suppressed SAPs at E12 by ≈3-fold, arguing that the current is rate-limiting for spontaneous Ca^{2+} spikes in early development and during regeneration. Because there was a stark association between the time of disappearance of the transient Ca^{2+} current and SAP, it is unlikely that the two events are unrelated. Moreover, at the later stages of embryonic development (e.g., E16–E17), the contribution of the transient Ca^{2+} current to the total Ca^{2+} current is nominal, and it is expected that the L-type Ca^{2+} current dominates mediation of Ca^{2+} spikes (34). The transition from spontaneously firing HCs to quiescent states may be derived not only from the coincidence expression of BK ($I_{K,f}$) and delayed rectifier K^+ current ($I_{K,n}$) (35, 36) but also from the developmental down-regulation of Ca^{2+} currents in HCs (37).

Ca^{2+} entry from T-type Ca^{2+} currents alone raises several possible scenarios for the developing and regenerating HCs, none of which is mutually exclusive. First, the low-threshold features of the current will amplify depolarizing inputs, promoting membrane excitability, and its inactivation may generate burst-firing patterns from tonic inputs. Consequently, a Ca^{2+} influx driven by a large tail current ensues to facilitate robust alteration of intracellular Ca^{2+} during activity. Second, overlap of the steady-state activation and inactivation relations at a potential range near the resting potential of HC, will create steady Ca^{2+} entry by virtue of a window current, resulting in a further boost of intracellular Ca^{2+} (38). Finally, the inactivation of the transient Ca^{2+} current may be self-limiting, creating a feedback control to prevent Ca^{2+} overload.

Regardless of the features of the T-type current, functional results showing that the expression of the current can mediate phasic changes in intracellular Ca^{2+} may prove to be an important requirement for the synthesis and release of neurotrophins during HC development and regeneration (9). The transcription and secretion of neurotrophins are stimulated preferentially by patterned electrical activity and the ensuing changes in Ca^{2+} transients, opposed to steady firing activity (39). Indeed, the expression of Trk neurotrophin receptors is regulated tightly by electrical activity, revealing a precise mechanism by which neurotrophins may selectively affect electrically active neurons (40). Specifically, in the inner ear,

there is a firm connection between the release of BDNF and neurotrophin 3 and the specificity of HC innervation in the cochlea. Apparently, neurotrophins may define the innervation pattern of type II afferents on outer HCs producing an apex-to-base preference gradient (41). Meanwhile, a relationship between the rate of rhythmic bursting and the tonotopic position of neurons within auditory nuclei has also been described in ref. 42. The pattern of spontaneous activity in CN may originate from inner hair cells (IHCs), as single patch–clamp recordings have shown, indirectly, that the firing properties of afferent terminals are correlated with spontaneous APs in IHCs (43). Thus, any positional and developmental differences in patterning and/or frequency of APs in IHCs are likely to be represented in the activity of the afferent fibers, potentially driving the refinement of synaptic connections within the cochlea and the central auditory system. It is conceivable that variations in the firing pattern of apical and basal HCs may selectively promote secretion of specific neurotrophins to confer the spatial pattern of innervation.

Another important corollary of the activity of HCs is neurotrophin-mediated neuronal survival. Null deletion of TrkB and TrkC receptors results in the loss of all spiral ganglion neurons (44). Previous studies have demonstrated that cochlea removal impacts CN neural survival and atrophy in neonatal and adult chickens as well as in other mammalian models (2), raising the intriguing assertion that there is a sustained trophic interaction between the cochlea and CN neurons. Nonetheless, there appears to be a critical window when removal of inputs from the cochlea induces robust cell death in the CN (45), suggesting that susceptibility to afferent deprivation may potentially depend on a molecular switch (46). Thus, the challenges for newly regenerated HCs are not only to establish a synaptic niche with spiral ganglion neurons but also to resume their position in the tonotopic map of the CN to mediate the survival of neurons. Resumption of SAPs in the regenerating HC may represent the first step in the process of synaptogenesis.

Materials and Methods

Isolation of the Chicken Basilar Papilla. Basilar papillae were isolated as described in ref. 47. All experiments were performed within 545 min of isolation (see *SI Experimental Procedures*).

Electrophysiology. Ca^{2+} currents and SAPs were recorded in whole-cell voltage–clamp configuration by using 3–5 MΩ resistance pipettes as described in refs. 8 and 12.

Data Analysis. Data were analyzed using pClamp8 (Axon Instruments) and Origin version 7.0 (Microcal Software). Differences between groups were tested using Student *t* tests, and the null hypothesis was rejected when the *P* value was <0.05. The *n*'s reported reflect the number of cells.

RT-PCR. Total RNA was extracted from microdissected basilar papilla of E8, E12, E16, and P1 chickens by using RNAlater (Ambion) and RNAeasy Mini Kit (Qiagen). Genomic DNA contamination was eliminated using RNase-free DNase treatment. RT-PCR was performed using TaqDNA Polymerase (Qiagen) and 1/20 of each cDNA preparation. All PCR products were then sequenced for identity confirmation.

Quantitative RT-PCR. Two-step quantitative real-time RT-PCR was performed using Brilliant SYBR green QRT-PCR reagents (Stratagene) by an ICycler IQ real-time PCR detection system (Bio-Rad).

***In Situ* Hybridization.** A 114-bp new exon specific to the long isoform of $Ca_v3.1$ was amplified using primers Ch1G-LF-qF and Ch1G-LF-qR and then subcloned into a pCRII-TOPO vector (Invitrogen).

Dr. Chiamvimonvat provided constructive comments on the manuscript, and Megan Yamoah helped in generating the figures. This work was supported by National Institutes of Health National Institute on Deafness and Other Communication Disorders Grants DC07592, DC03826 (both to E.N.Y.), and DC04295 (to B.H.A.S.) and by a grant from the National Organization for Hearing Research (to S.L.).

1. McLaughlin T, Torborg CL, Feller MB, O'Leary DD (2003) *Neuron* 40:1147–1160.
2. Born DE, Rubel EW (1985) *J Comp Neurol* 231:435–445.
3. Saunders JC, Adler HJ, Cohen YE, Smullen S, Kazahaya K (1998) *J Comp Neurol* 390:412–426.
4. Corwin JT, Cotanche DA (1988) *Science* 240:1772–1774.
5. Lippe W (1994) *J Neurosci* 14:1486–1495.
6. Jones TA, Jones SM, Paggett KC (2001) *J Neurosci* 21:8129–8135.
7. Meister M, Wong RO, Baylor DA, Shatz CJ (1991) *Science* 252:939–943.
8. Marcotti W, Johnson SL, Rusch A, Kros CJ (2003) *J Physiol (London)* 552:743–761.
9. Eatock RA, Hurley KM (2003) *Curr Top Dev Biol* 57:389–448.
10. Spitzer NC (2002) *J Physiol (Paris)* 96:73–80.
11. Kollmar R, Fak J, Montgomery LG, Hudspeth AJ (1997) *Proc Natl Acad Sci USA* 94:14889–14893.
12. Rodriguez-Contreras A, Yamoah EN (2001) *J Physiol (London)* 534:669–689.
13. Bao H, Wong WH, Goldberg JM, Eatock RA (2003) *J Neurophysiol* 90:155–164.
14. Platzer J, Engel J, Schrott-Fischer A, Stephan K, Bova S, Chen H, Zheng H, Striessnig J (2000) *Cell* 102:89–97.
15. Katayama A, Corwin JT (1989) *J Comp Neurol* 281:129–135.
16. Martinez-Dunst C, Michaels RL, Fuchs PA (1997) *J Neurosci* 17:9133–9144.
17. Si F, Brodie H, Gillespie PG, Vazquez AE, Yamoah EN (2003) *J Neurosci* 23:10815–10826.
18. Whitehead MC, Morest DK (1985) *Neuroscience* 14:255–276.
19. Saunders JC, Coles RB, Richard Gates G (1973) *Brain Res* 63:59–74.
20. Chuang RS, Jaffe H, Cribbs L, Perez-Reyes E, Swartz KJ (1998) *Nat Neurosci* 1:668–674.
21. Monteil A, Chemin J, Leuranguer V, Altier C, Mennessier G, Bourinet E, Lory P, Nargeot J (2000) *J Biol Chem* 275:16530–16535.
22. Ryals BM, Rubel EW (1988) *Science* 240:1774–1776.
23. Stone JS, Rubel EW (2000) *Proc Natl Acad Sci USA* 97:11714–11721.
24. Llinas R, Yarom Y (1981) *J Physiol (London)* 315:549–567.
25. Fuchs PA, Sokolowski BH (1990) *Proc Biol Sci* 241:122–126.
26. Wooltorton JR, Gaboyard S, Hurley KM, Price SD, Garcia JL, Zhong M, Lysakowski A, Eatock RA (2007) *J Neurophysiol* 97:1684–1704.
27. Fuchs P, Nagai T, Evans M (1988) *J Neurosci* 8:2460–2467.
28. Martini M, Rossi ML, Rubbini G, Rispoli G (2000) *Biophys J* 78:1240–1254.
29. Rodriguez-Contreras A, Nonner W, Yamoah EN (2002) *J Physiol (London)* 538:729–745.
30. Rennie KJ, Ashmore JF (1991) *Hear Res* 51:279–291.
31. Gu X, Spitzer N (1993) *J Neurosci* 13:4936–4948.
32. Chambard JM, Chabbert C, Sans A, Desmadryl G (1999) *J Physiol (London)* 518:141–149.
33. Chameau P, Lucas P, Melliti K, Bournaud R, Shimahara T (1999) *Neuroscience* 90:383–388.
34. Beutner D, Moser T (2001) *J Neurosci* 21:4593–4599.
35. Lawlor P, Marcotti W, Rivolta MN, Kros CJ, Holley MC (1999) *J Neurosci* 19:9445–9458.
36. Oliver D, Knipper M, Derst C, Fakler B (2003) *J Neurosci* 23:2141–2149.
37. Roux I, Safieddine S, Nouvian R, Grati M, Simmler MC, Bahloul A, Perfettini I, Le Gall M, Rostaing P, Hamard G, *et al.* (2006) *Cell* 127:277–289.
38. Barish ME, Mansdorf NB (1991) *Dev Brain Res* 63:53–61.
39. Balkowiec A, Katz DM (2002) *J Neurosci* 22:10399–10407.
40. McAllister AK, Katz LC, Lo DC (1996) *Neuron* 17:1057–1064.
41. Farinas I, Jones KR, Tessarollo L, Vigers AJ, Huang E, Kirstein M, de Caprona DC, Coppola V, Backus C, Reichardt LF, Fritzsch B (2001) *J Neurosci* 21:6170–6180.
42. Lippe WR (1995) *Brain Res* 703:205–213.
43. Glowatzki E, Fuchs PA (2002) *Nat Neurosci* 5:147–154.
44. Schimmang T, Alvarez-Bolado G, Minichiello L, Vazquez E, Giraldez F, Klein R, Represa J (1997) *Mech Dev* 64:77–85.
45. Tierney TS, Russell FA, Moore DR (1997) *J Comp Neurol* 378:295–306.
46. Mostafapour SP, Del Puerto NM, Rubel EW (2002) *J Neurosci* 22:4670–4674.
47. Zhao Y, Yamoah EN, Gillespie PG (1996) *Proc Natl Acad Sci USA* 93:15469–15474.